Reversible thermochromism of $CsPbBr_3$ - doped tellurite glass

Luyue Niu [1, 2], Lu Wang [1, 2], Ying Ye [3], Ruilin Zheng [4], Wenhao Li [1, 2], Jiayue Yang [4], Chao Liu [3], Lu Liu [1, 2], Xiaoxin Zheng [1, 2,a)], Jing Ren [1, 2, a)], Jianzhong Zhang[1, 2]

AFFILIATIONS

[1] Key Lab of In-fiber Integrated Optics, Ministry Education of China, Harbin Engineering University, Harbin 150001, China

[2] Key Laboratory of Photonic Materials and Devices Physics for Oceanic Applications, Ministry of Industry and Information Technology of China, College of Physics and Optoelectronic Engineering, Harbin Engineering University, Harbin 150001, China

[3] State Key Laboratory of Silicate Materials for Architectures, Wuhan University of Technology, Wuhan 430070, China

[4] College of Science, Nanjing University of Posts and Telecommunications, Nanjing 210023, China

[5] School of Energy and Power Engineering, Shandong University, Jinan, Shandong 250061, China

Corresponding authors

[a)] Authors to whom correspondence should be addressed: xxzheng@hrbeu.edu.cn and ren.jing@hrbeu.edu.cn

Experimental Section

The microstructure of PQDs-doped glass is implemented by using a Cs-corrected JEOL 2200FS transmission electron microscope (TEM). Bright-/dark-field TEM, high-resolution TEM (HR-TEM) and high-angle-annular-dark-field STEM (HAADF-STEM) images were measured using a FEI Talos F200X operating at an acceleration voltage of 200 kV and equipped with an energy-dispersive spectrometer (EDS). TEM samples with a thickness of approximately 50 nm were prepared by ion-beam milling using a PIPS system from GATAN. In the STEM-EDS elemental mapping measurement, the probe size was 0.13 nm in diameter, the examined area (~ 120 × 120 nm^2) was divided into 2048 × 2048 pixels, and the dwell time was 20 μs per pixel. It took approximately 20 s per frame and 80 s to acquire a mapping image.

Variable temperature transmission spectrum detection of specimens is made by a UV-Vis-NIR spectrometer (Lambda 750s, PerkinElmer, USA) with vacuum optical windows and heating plates. During variable-temperature XRD testing, a heating stage or temperature control system is introduced into the X-ray diffractometer (Bruker D8 Venture; Rigaku Smart Lab, Japan) to monitor how the crystal structure of the sample changes with temperature. For variable-temperature XPS testing, the chemical state and electronic structure of the sample surface are monitored as the temperature of the reaction chamber is varied from room temperature to 573 K. The

sample is placed in a temperature - controlled reaction chamber connected to the XPS instrument (Kratos Axis Supra a TM; Thermo ESCALAB 250XI). Raman spectroscopy measurements at varying temperatures are conducted using a Raman spectrometer (LabRAM HR 800 by Horiba, Canada), analyzing the molecular vibrational modes and crystal structure of the material as the temperature changes from room temperature to 673 K. The refractive index is measured using a state-of-the-art infrared variable-angle spectroscopic ellipsometer (IR - VASE), with a spectral range of 400 - 700 cm^{-1}. As the temperature changes (from RT to 573K), the density and molecular arrangement of the material will alter, leading to variations in the refractive index and providing insights into the material's thermos - optical properties, and the specific measurement process is described in the work of Yang et al [1,2]. In all variable - temperature tests, the measurements are conducted after allowing the sample to stabilize for 10 minutes at each temperature point.

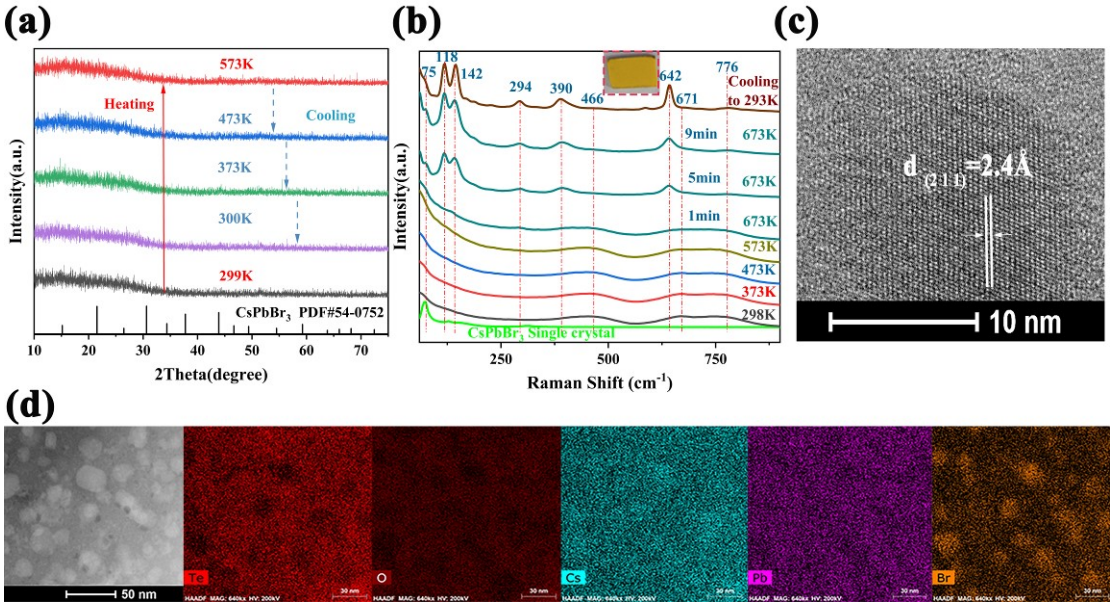

Fig. S1. (a) XRD pattern and (b) Raman curves of the $CsPbBr_3$ PQDs-doped glass (GC samples) at different temperature, 1min, 5min, and 9min represent the duration for which the sample is maintained at 673K (c) HRTEM image of a single $CsPbBr_3$ PQD embedded in tellurite glass (d)TEM images of the $CsPbBr_3$ PQDs - doped glass precipitated at 340°C/15h. The inset of (b): a photograph of the sample cooled to room temperature after being heated to 673K.

Figure S1(a) presents the temperature-dependent XRD tests of $CsPbBr_3$ PQDs composite glass (GC), where no obvious peaks corresponding to the perovskite or other crystalline phases were detected even after the glass sample underwent heat treatment at 613 K (340°C) for 15 hours. The Raman spectra (Figure S1 (b)) revealed

that the characteristic peak of the $CsPbBr_3$ mode at 75 cm^{-1} corresponds to the vibrational mode of the $[PbBr_6]^{4-}$ octahedron, while the modes at 118 and 142 cm^{-1} are attributed to the transverse optical (TO) and longitudinal optical (LO) phonons, corresponding to the stretching vibrations of Pb - Br. The mode at 294 cm^{-1} is associated with the second-order phonon mode [3]. The characteristic vibrational peaks at 466 cm^{-1} and 671 cm^{-1} represent the non-axial Te - O - Te bending vibrations and axial Te - O - Te stretching vibrations of the $[TeO_{3+1}]$ group, respectively. The vibration at 776 cm^{-1} corresponds to the Te - O stretching vibrations within the $[TeO_4]$ group. Within the temperature range of 293 K to 573 K, all Raman modes exhibited relatively weak intensities. However, when the temperature was raised to 673 K, a significant enhancement in the intensity of the Raman modes observed for the $CsPbBr_3$ crystals was noted. Concurrently, as the dwell time at this temperature increased, the full width at half maximum (FWHM) of the maximum peak narrowed, and the peak intensity increased. At this point, the test temperature had surpassed the crystallization temperature of the tellurite glass used in this study, leading to excessive crystallization of the glass, particularly the tellurite glass matrix. Direct evidence for the formation of $CsPbBr_3$ perovskite quantum dots (PQDs) is provided by high-resolution transmission electron microscopy (HRTEM) images, as shown in Figure S1(c). The single-crystal nature of the PQDs, with clearly resolved lattice fringes, is confirmed, revealing an interplanar spacing of 0.24 nm, which corresponds to the d (2 1 1) plane of $CsPbBr_3$. The corresponding TEM image reveals that the PQDs particles can be seen distributing in the glass matrix without aggregation, and the elemental mapping shows the PQDs are enriched with Cs and Br and excluded from glass matrix (Te and O) (Fig S1(d)).

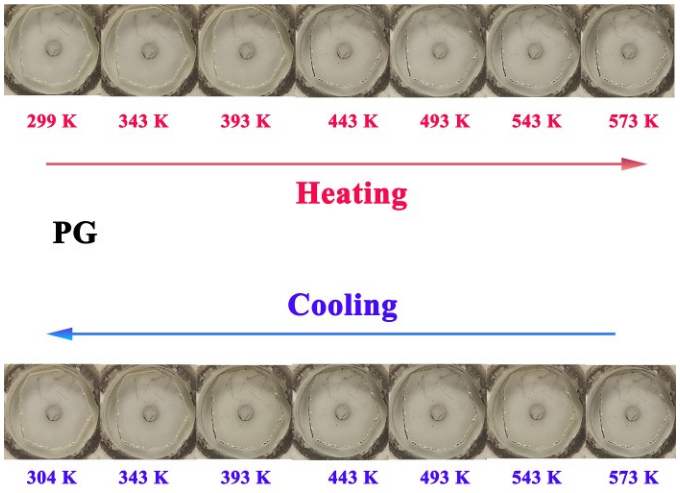

Fig S2. the PG sample pictures at different temperature.

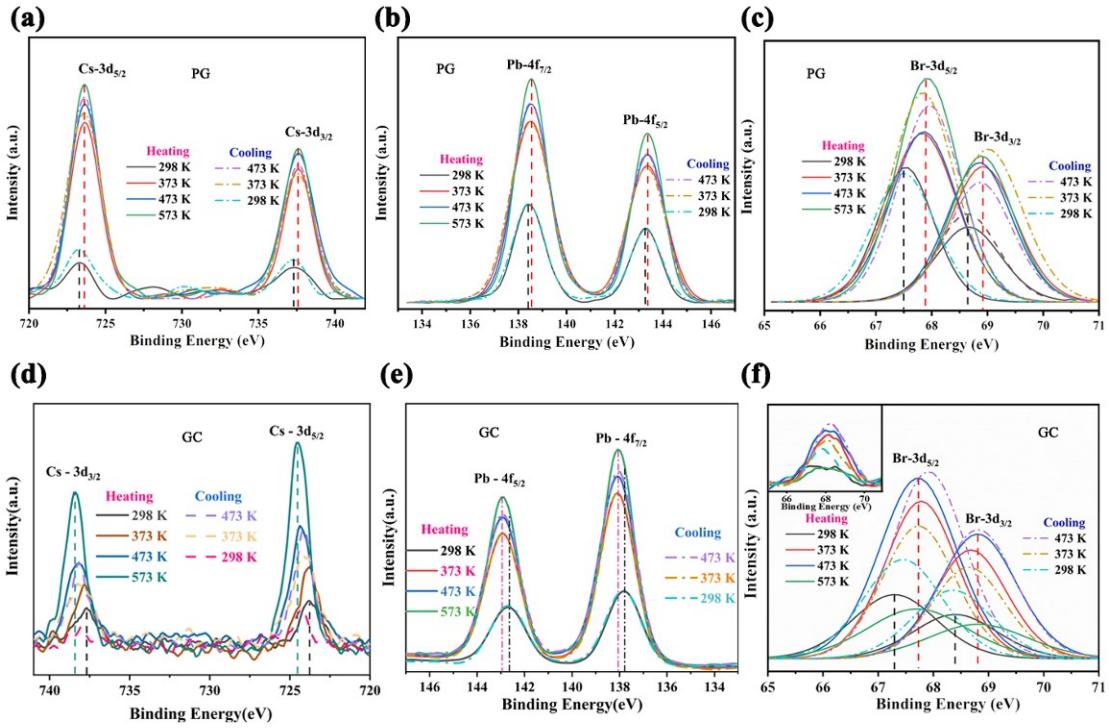

Fig. S3. Temperature dependent core-level XPS scan of the(a) (d) Cs 3d, (b) (e) Pb 4f (c) (f) Br 3d of the precursor glass (PG) and thermally - treated (GC) glasses. Insert of (c): the origin XPS scan of Br-3d with unattributed peaks.

Table S1. Binding Energy (eV) of Cs 3d, Pb 4f and Br 3d for PG and GC samples at 298 K.

	Cs-3d$_{5/2}$	**Cs-3d$_{3/2}$**	**Pb-4f$_{7/2}$**	**Pb-4f$_{5/2}$**	**Br-3d$_{5/2}$**	**Br-3d$_{3/2}$**
PG	723.3 eV	737.4 eV	138.4 eV	143.3 eV	67.5 eV	68.6 eV

GC	723.7 eV	737.7 eV	137.8 eV	142.7 eV	67.3 eV	68.4 eV

Table S2. Binding Energy (eV) shifts of Cs 3d, Pb 4f and Br 3d for PG and GC samples from 298 K to 573 K.

	Cs-3$d_{5/2}$	**Cs-3$d_{3/2}$**	**Pb-4$f_{7/2}$**	**Pb-4$f_{5/2}$**	**Br-3$d_{5/2}$**	**Br-3$d_{3/2}$**
PG	0.3 eV	0.2 eV	0.1 eV	0.1 eV	0.4 eV	0.3 eV
GC	0.8 eV	0.7 eV	0.2 eV	0.2 eV	0.4 eV	0.4 eV

The X-ray photoelectron spectroscopy (XPS) analysis of GC and PG samples reveals distinctive peaks for Cs^+, Pb^{2+}, and Br^-, as depicted in Fig. S3 and detailed in Table S1-S2.

In detail, Table S1 provides a comparative analysis of peak positions at room temperature (298 K) for PG and GC samples, revealing shifts that signify alterations in the chemical environment of the respective elements. For instance, the binding energy of Pb^{2+} transitions from 138.4 eV (Pb-4$f_{7/2}$) and 143.3 eV (Pb-4$f_{5/2}$) in PG samples to 137.8 eV (Pb-4$f_{7/2}$) and 142.7 eV (Pb-4$f_{5/2}$) in GC samples. This shift is likely attributable to the formation of $CsPbBr_3$ perovskite quantum dots (PQDs) in the GC samples, which may modify the coordination environment of Pb^{2+} by substituting Pb-O bonds in the PG sample with Pb-Br bonds or by diminishing the Pb-Br bond distance. Such modifications likely enhance the electron density around the Pb atom, thereby lowering the binding energy of Pb^{2+}.[4-8] Conversely, the binding energies of Cs and Br exhibit only minor variations, possibly due to their simpler electronic structures and coordination environments.

Furthermore, the binding energies of these peaks demonstrate analogous reversible shifts with temperature variations for both PG and GC samples. As illustrated in Fig. S3, an increase in temperature prompts the characteristic peaks for Cs, Pb, and Br to shift towards higher binding energies, with subsequent cooling causing these peaks to revert to lower binding energies. This behavior is attributed to the thermal expansion of the material structure at high temperatures, which results in longer bond lengths and reduced electron cloud density of the corresponding elements. Specifically, the thermal expansion coefficient for tellurite glass is approximately 17×10^{-6} K^{-1}, while for cubic $CsPbBr_3$ crystal, it is about 33×10^{-6} K^{-1}. Thus, elements in the GC are more markedly influenced by temperature, exhibiting more pronounced peak shifts compared to PG (Table S2). Additionally, the development of Pb-O, Cs-O, and Br-O bonds resulting from ionic migration may also contribute to this effect. Pb^{2+} ions, due to their relatively stable coordination environment, show less temperature-induced variation, whereas Cs ions, located in interstitial sites within the $CsPbBr_3$ crystal structure, are more sensitive to temperature fluctuations. The Br element displays intermediate behavior.

Significantly, at 573 K, an observable increase in Cs concentration in the GC sample is noted, likely attributable to Cs migrating to the surface as the glass viscosity decreases near the glass transition temperature of 599 K. This migration elevates the surface concentration of Cs. In contrast, the concentration of Br diminishes,

suggesting a migration of Br towards the interior of the material. Pb, which generally occupies a more stable position, exhibits minimal diffusion at elevated temperatures. This ionic migration consequently leads to a surface charge imbalance. Honestly, we are currently unable to fully elucidate the underlying mechanisms driving this migration.

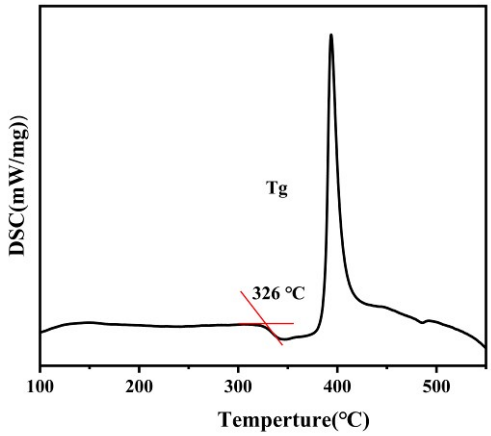

Fig. S4. DSC curves of the PG samples

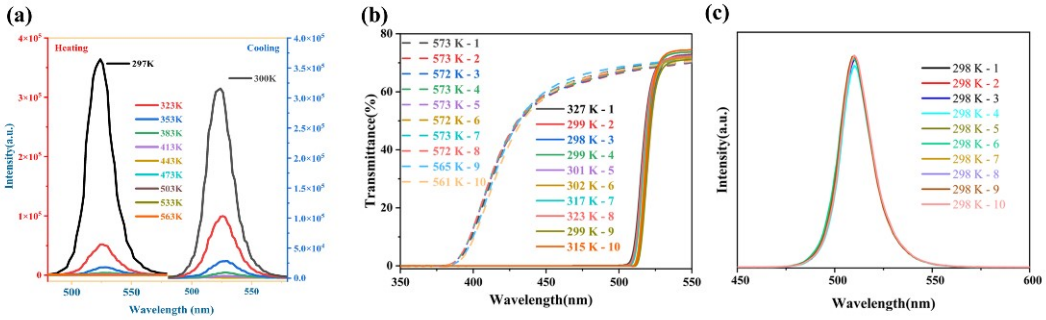

Fig S5 (a) Temperature dependent photoluminescence spectra of PQDs doped glass (GC) recorded with 410 nm emitting diode laser as excitation source; (b) Temperature dependent transmittance spectra and (b) PL (λ_{ex}=410nm) spectra under multiple reversible process (10 Cycles)

As shown in Fig S5(a), during heating, the fluorescence intensity notably decreased until it completely disappeared at about 413 K. Correspondingly, during cooling, the luminescence of GC gradually recovered, indicating reversible emission during temperature cycling. Furthermore, due to the thermal relaxation effect, luminescence at the same temperature differs between heating and cooling. Comparing with the transmittance profile of GC, which shows thermochromism at 543 K (270°C) during heating and 393 K (120°C) during cooling, the luminescence shows similar trends. It is noteworthy that there is a significant difference in the luminescence intensity of the sample at 300K and 297K, despite just a 3K temperature difference, highlighting the

sensitivity of perovskite quantum dots to temperature changes. Accordingly, we precisely controlled the test temperature to 298K after the temperature cycling and obtained the photoluminescence results shown in Fig S5(c), accurately characterizing the reversibility of the luminescence of GC.

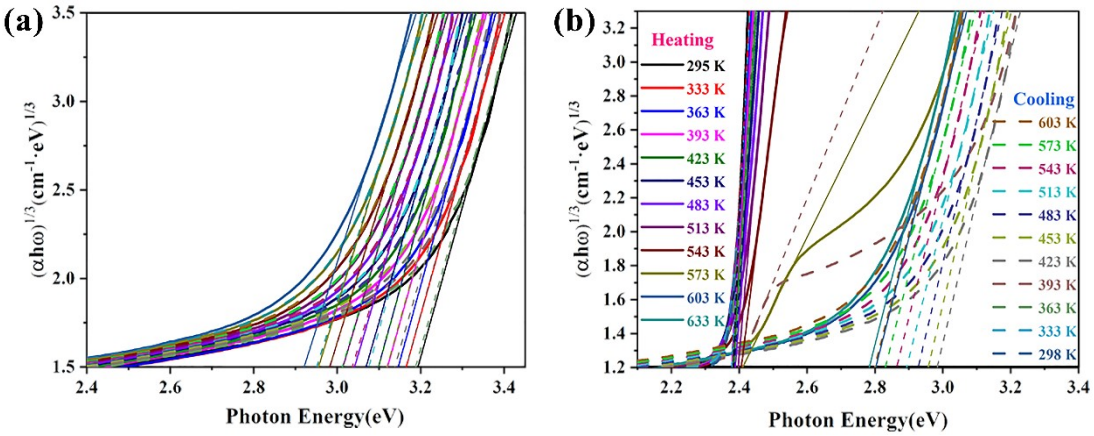

Fig.S6 The light energy of (a) PG and (b) GC samples vary with photon energy at different temperatures.

Depending on the nature of the electronic transition during absorption, the value of p can be 1/2, 3/2, 2, or 3, corresponding to allowed direct transitions (p=1/2), forbidden direct transitions (p=3/2), allowed indirect transitions (p=2), and forbidden indirect transitions (p=3), respectively. For amorphous glass materials, according to the Tauc relation, indirect transitions are generally effective, hence this study takes p as 3.

Table S3 Values of band gap energy of PG sample at different temperatures.

Temperature (K)		**293**	**297**	**333**	**363**	**393**	**423**	**453**	**483**	**513**	**543**	**573**	**603**
E_g (eV)	Heating	3.19	--	3.17	3.13	3.1	3.08	3.05	3.02	2.99	2.96	2.93	2.90
	Cooling		3.19	3.16	3.12	3.10	3.08	3.04	3.01	2.99	2.96	2.93	
lnα	Heating	3.97	--	3.86	3.78	3.78	3.82	3.75	3.60	3.48	3.43	3.36	3.27
	Cooling		3.75	3.80	3.88	3.85	3.88	3.78	3.54	3.47	3.43	3.36	
E_u (eV)	Heating	0.25	--	0.26	0.26	0.26	0.26	0.27	0.28	0.29	0.29	0.30	0.31
	Cooling		0.27	0.26	0.26	0.26	0.26	0.26	0.28	0.29	0.299	0.30	

Table S4 Values of band gap energy of GC sample at different temperatures.

Temperature	**295**	**298**	**333**	**363**	**393**	**423**	**453**	**483**	**513**	**543**	**573**	**603**	**633**

(K)														
E_g (eV)	Heating	2.38	--	2.38	2.38	2.38	2.38	2.39	2.39	2.40	2.41	2.59	2.80	2.78
	Cooling	--	2.38	2.38	2.39	2.79	2.98	2.96	2.93	2.89	2.86	2.83	2.80	
lnα	Heating	21.54	--	19.01	17.27	15.90	14.38	13.19	12.09	10.88	8.92		3.69	3.65
	Cooling	--	21.43	18.94	16.57		4.02	3.95	3.89	3.80	3.76	3.63	3.55	
E_u (eV)	Heating	0.05	0.05	0.06	0.06	0.06	0.07	0.08	0.08	0.09	0.11		0.27	0.27
	Cooling	--	0.05	0.05	0.06		0.25	0.25	0.26	0.26	0.27	0.28	0.28	

Table. S5 Data of the temperature-induced bandgap change rate （fitting parameter α through Varshni equation） for various group semiconductors, tellurite glass perovskites and perovskite glass.

Materials	semiconductor				Tellurate matrix glass		
	GaAs	InAs	InP	GaP	Te - W - Li	Te - Na	Te - Ga - Zn
bandgap （$MeVK^{-1}$）	-0.887, -0.58, -0.541	-0.316	-0.491	-0.557	-0.4 – -0.9	-0.6 – -0.9	0.95

Materials	Lead-free perovskite		Lead based perovskite		$CsPbBr_3$ PQDs doped glass	
	$Cs_2AgSbCl_5$	$Cs_2NaFeCl_6$	$CsPbBr_3$	$MAPbBr_3$	Si - $CsPbBr_3$	Te - $CsPbBr_3$
bandgap change rate（$MeVK^{-1}$）	-2.52	-0.837	-0.34	-0.257	1.55	1.37

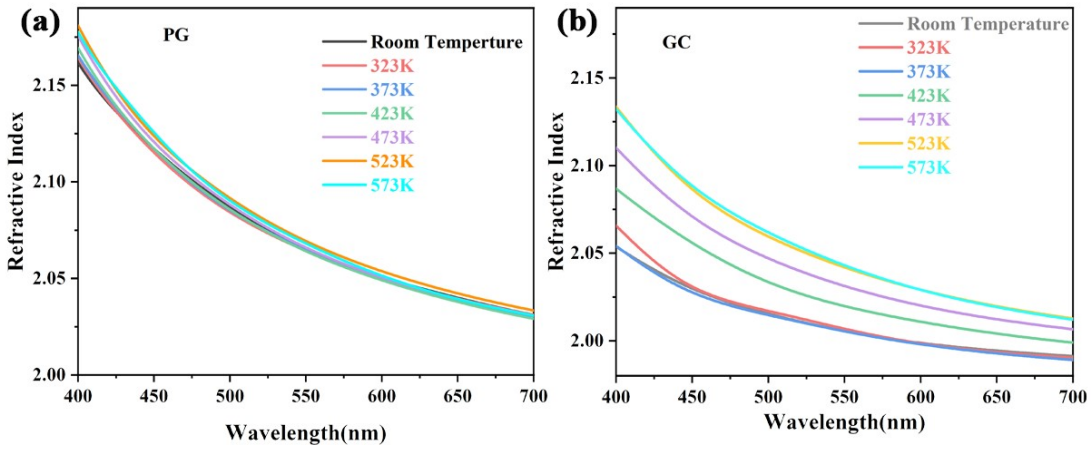

Fig. S7 Refractive index versus wavelength of (a) PG and (b) GC samples varies with temperatures.

The refractive index and its temperature dependence (i.e., the thermo-optic coefficient (dn/dT) are fundamental optical parameters for optical materials, including glass, and hold significant practical importance in numerous optical and optoelectronic applications such as focusing, guiding, coupling, radiation modulation, and fiber optic communication systems.

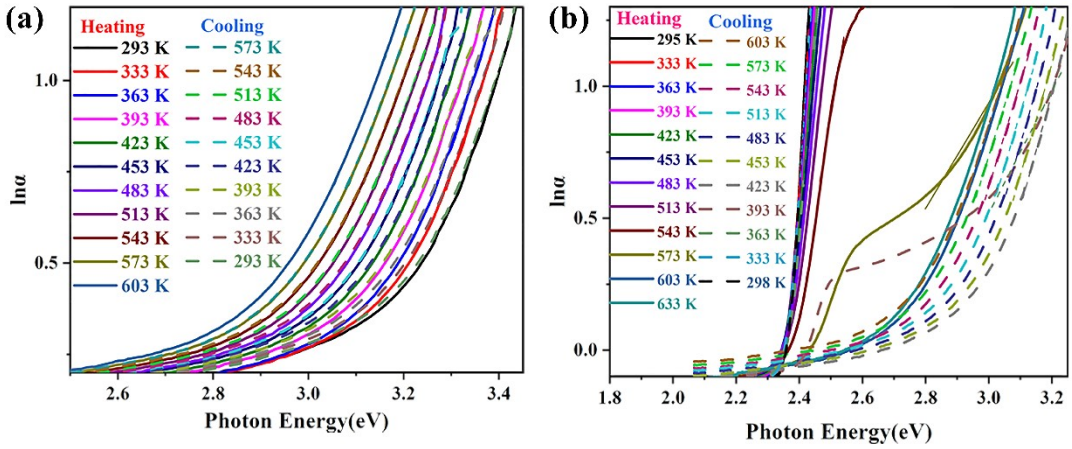

Fig. S8 lnα of （a） PG and （b） GC samples vary with photon energy at different temperatures.

The presence of tail states in amorphous solids has a profound impact on band-to-band light absorption. Unlike crystalline solids, intrinsic absorption in amorphous solids can also occur within the photon energy range below the mobility gap. All amorphous semiconductors and insulators appear to exhibit the same characteristic absorption behavior in this energy gap region, known as the Urbach energy. The Urbach energy is an indicator that describes the tail of the band in amorphous or locally ordered materials, representing the static and dynamic disorder within a

semiconductor, which can be directly obtained through optical characterization techniques. This relationship was initially observed in ionic crystals (particularly AgBr used as photographic emulsions)，As the incompleteness and heterogeneity of the local structure increase (the greater the disorder), the Urbach edge becomes less steep (smaller), leading to an increase in the width of the Urbach tail, and consequently, an increase in the Urbach energy. The exponential energy dependence of the Urbach edge seems to be due to the exponential energy distribution of the band tail states.

REFERENCES

[1] J.Y. Yang, W.J. Zhang, L.H. Liu, J. Qiu, K. Wang, and J.Y. Tan, "Temperature-dependent infrared dielectric functions of MgO crystal: An ellipsometry and first-principles molecular dynamics study," J. Chem. Phys. **141**(10), 104703 (2014).

[2] T. Cheng, T. Fei, W. Zhang, J.-Y. Yang, and L. Liu, "Ellipsometric and first-principles study on temperature-dependent UV–Vis dielectric functions of GaN," Appl. Opt. **60**(23), 6869 (2021).

[3]Z. Zhao, M. Zhong, W. Zhou, Y. Peng, Y. Yin, D. Tang, and B. Zou, "Simultaneous Triplet Exciton–Phonon and Exciton–Photon Photoluminescence in the Individual Weak Confinement $CsPbBr_3$ Micro/Nanowires," J. Phys. Chem. C **123**(41), 25349–25358 (2019).

[4] K.J. Babu, G. Kaur, L. Biswal, G. De, and H.N. Ghosh, "Ultrafast Charge Delocalization Dynamics of Ambient Stable $CsPbBr_3$ Nanocrystals Encapsulated in Polystyrene Fiber," Chem. – Eur. J. **27**(2), 683–691 (2021).

[5] Y. Jiang, L. Yang, G. Liang, S. Liu, W. Gao, Z. Yang, X. Wang, R. Lin, and X. Zhu, "The poisoning effect of PbO on CeO_2-MoO_3/TiO_2 catalyst for selective catalytic reduction of NO with NH_3," Mol. Catal. **486**, 110877 (2020).

[6] H. An, Z. Gao, X. Zhao, and Y. Wang, "MgO-PbO Catalyzed Synthesis of Diethylene Glycol Bis(allyl carbonate) by Transesterification Route," Ind. Eng. Chem. Res. **50**(13), 7740–7745 (2011).

[7] L.R. Pederson, "Two-dimensional chemical-state plot for lead using XPS," J. Electron Spectrosc. Relat. Phenom. **28**(2), 203–209 (1982).

[8] L. Zhou, C. Li, L. Zhao, G. Zeng, L. Gao, Y. Wang, and M. Yu, "The poisoning effect of PbO on Mn-Ce/TiO_2 catalyst for selective catalytic reduction of NO with NH3 at low temperature," Appl. Surf. Sci. **389**, 532–539 (2016).